ATMOSPHERIC SCIENCE

Rapid rise in premature mortality due to anthropogenic air pollution in fast-growing tropical cities from 2005 to 2018

Karn Vohra[1,2]*, Eloise A. Marais[2]*, William J. Bloss[1], Joel Schwartz[3], Loretta J. Mickley[4], Martin Van Damme[5], Lieven Clarisse[5], Pierre-F. Coheur[5]

Tropical cities are experiencing rapid growth but lack routine air pollution monitoring to develop prescient air quality policies. Here, we conduct targeted sampling of recent (2000s to 2010s) observations of air pollutants from space-based instruments over 46 fast-growing tropical cities. We quantify significant annual increases in nitrogen dioxide (NO_2) (1 to 14%), ammonia (2 to 12%), and reactive volatile organic compounds (1 to 11%) in most cities, driven almost exclusively by emerging anthropogenic sources rather than traditional biomass burning. We estimate annual increases in urban population exposure to air pollutants of 1 to 18% for fine particles ($PM_{2.5}$) and 2 to 23% for NO_2 from 2005 to 2018 and attribute 180,000 (95% confidence interval: −230,000 to 590,000) additional premature deaths in 2018 (62% increase relative to 2005) to this increase in exposure. These cities are predicted to reach populations of up to 80 million people by 2100, so regulatory action targeting emerging anthropogenic sources is urgently needed.

INTRODUCTION

More than 40% of the global population resides in the tropics (*1*). Of those, less than half reside in urban areas, although this is expected to exceed 50% by 2050 because of steep rates of urbanization and unprecedented population growth (*1*). By 2100, most (51 of 70) global megacities are projected to be in the tropics (25°S to 25°N), concentrated in Africa and Asia (*2*). This has the potential for severe impacts on air quality and climate, as megacities represent an overwhelming contribution to carbon and air pollutant emissions (*3*, *4*). Many countries in the tropics have yet to implement robust policies and necessary infrastructure to monitor and mitigate air pollution (*5*). Even where policies exist, such as in large cities in India, there is limited evidence of remediation (*6*). Knowledge of recent trends in the sources, abundance, and population exposure to air pollution in these rapidly growing cities is crucial for demonstrating the scale of air quality degradation and to hasten adoption of sustainable mitigation measures to avoid repeating past air pollution health crises.

Ambient air pollution in much of the tropics is dominated by widespread, intense seasonal open burning of biomass (*7*, *8*). The contribution from anthropogenic activity varies regionally and is greatest in tropical Asia, predominantly from residential combustion and industrial activity (*7*, *9*). Air pollution in tropical Africa is also influenced by natural sources (desert dust and biogenic emissions) as well as residential and commercial production and use of solid fuels (*10*–*12*). Seasonality in meteorology affects air quality, particularly in West Africa (*13*) and India (*14*), where southwesterly winds and heavy rainfall during the monsoon season disperse and wash away pollution and stagnant conditions during the dry season lead to its accumulation. Combined rapid growth in anthropogenic activity and very efficient tropical deep convective injection of pollutants and precursors to the free troposphere also have the potential to greatly influence global atmospheric chemistry and climate (*15*). The relative role of natural, anthropogenic, and biomass burning sources to trends in air pollution in the tropics remains elusive (*7*, *16*, *17*).

Exposure to ambient fine particulate pollution ($PM_{2.5}$) is already a leading environmental health risk in many countries in the tropics (*5*, *18*). More than 30% of premature deaths in Asia are attributable to exposure to $PM_{2.5}$ from fossil fuel combustion alone (*19*), and 170,000 global premature infant deaths, mostly in South Asia and sub-Saharan Africa, have been attributed to exposure to $PM_{2.5}$ (*20*). Annual mean population-weighted $PM_{2.5}$ concentrations for the tropics are almost five times the recently updated World Health Organization (WHO) guideline of 5 μg m^{-3} (*21*), although this was determined with very few measurements (<1 monitor per million people in many tropical countries) (*22*). Monitoring capacity has improved with deployment of low-cost sensors and additional reference-grade instruments (*23*, *24*), but large data gaps as well as data quality and access issues remain. India, for example, has an extensive network of monitors operated and maintained by local and national authorities as well as research institutions, but the use of these for informing policies is hindered by data quality issues for the national network (*6*, *23*) and restricted access to data collected by research institutions and state governments.

Satellite observations provide long-term, consistent, global observations of a range of chemical components of the atmosphere. These offer constraints on long-term changes in abundance of surface air pollutants, precursor emissions of short-lived air pollutants (*25*, *26*), and sensitivity of ozone formation to source types for informing policy measures to regulate already severe ozone pollution in the tropics (*8*). Past studies have typically focused on a single pollutant observable from space-based sensors over current megacities, mostly in the northern hemisphere (*27*–*29*). Many fast-growing tropical cities are anticipated to reach 40 million to 80 million inhabitants

[1]School of Geography, Earth, and Environmental Sciences, University of Birmingham, Birmingham, UK. [2]Department of Geography, University College London, London, UK. [3]Department of Environmental Health, Harvard T.H. Chan School of Public Health, Harvard University, Boston, MA, USA. [4]John A. Paulson School of Engineering and Applied Sciences, Harvard University, Cambridge, MA, USA. [5]Université libre de Bruxelles (ULB), Spectroscopy, Quantum Chemistry and Atmospheric Remote Sensing (SQUARES), Brussels, Belgium.
*Corresponding author. Email: e.marais@ucl.ac.uk (E.A.M.); k.vohra@ucl.ac.uk (K.V.)

by 2100 (*2*), far greater than the 10 largest contemporary megacities of 20 million to 40 million (*1*). In our previous work, we demonstrated that space-based observations of integrated columns of nitrogen dioxide (NO_2) and ammonia (NH_3) abundances as well as aerosol optical depth (AOD) reproduce long-term trends in surface observations of NO_2, NH_3, and $PM_{2.5}$, respectively (*6*). Column abundances of formaldehyde (HCHO), a ubiquitous oxidation product of volatile organic compounds (VOCs), provide constraints on reactive VOCs (*30*).

Here, we conduct targeted sampling of more than a decade of satellite observations of NO_2, NH_3, AOD, and HCHO over fast-growing tropical cities to determine recent (2000s to 2010s) trends in air pollution abundance and precursor emissions and to discern the relative role of traditional and emerging pollution sources. We go on to estimate the increase in urban population exposure to the hazardous pollutants $PM_{2.5}$ and NO_2 and the associated health burden of exposure to $PM_{2.5}$ using a health risk assessment model constrained with epidemiological data representative of the range of $PM_{2.5}$ concentrations in the tropics.

RESULTS

Trends in air quality in fast-growing tropical cities

The 46 cities in tropical Africa, the Middle East, and Asia that are projected to be megacities (population ≥ 10 million) by 2100 are shown in Fig. 1. Only 12 are megacities now, mostly in India. Forecast population growth rates from 2020 to 2100 range from 3 to 31% per year (a^{-1}) in Africa, 1% a^{-1} for Riyadh and 8% a^{-1} for Sana'a in the Middle East, 0.8 to 3% a^{-1} in South Asia, and 0.5 to 7% a^{-1} in Southeast Asia (*2*). The largest cities, predicted to surpass 50 million inhabitants by 2100, include Lagos (80 million) in Nigeria, Dar es Salaam (62 million) in Tanzania, Kinshasa (60 million) in the Democratic Republic of the Congo, and Mumbai (58 million) in India. There are also five cities in tropical America that are already megacities (fig. S1), but our focus is on the cluster of tropical cities in Asia, Africa, and the Middle East because of their much faster projected growth (*2*).

Figure 2 shows trends in the short-lived pollutants NO_2 for 2005–2018, NH_3 for 2008–2018, and HCHO as a proxy for reactive nonmethane VOCs (NMVOCs) for 2005–2018 over these cities obtained from a long-term, consistent record of satellite observations (Table 1). Data processing to isolate the reactive component of the HCHO column is detailed in Materials and Methods. NO_2 increases in almost all (41) cities, by 0.1 to 14.1% a^{-1}. The increase is significant for 34 of these 41 cities (Fig. 2A) and has the potential to lead to increases in $PM_{2.5}$ by forming aerosol nitrate. NO_2 triples over Chittagong (Bangladesh) and more than doubles over Antananarivo (Madagascar), Hanoi (Vietnam), Luanda (Angola), and Dhaka (Bangladesh). NO_2 declines in five cities, although the downward trend is only appreciable and significant for Jakarta (−2.0% a^{-1}). This decline, already identified using an earlier record of observations from the same satellite instrument (*25*, *31*), likely reflects emission controls imposed on vehicles since 2005 (*25*, *32*). The record of NO_2 for cities in Africa starts at ~60% lower values than Asian cities, due to prevalence of inefficient combustion sources with relatively low NO_x emissions across Africa (*10*). In general, upward trends in NO_2 cover a similar range in Africa (0.3 to 8.2% a^{-1}) and Asia (0.8 to 7.7% a^{-1}, excluding 14.1% a^{-1} for Chittagong). The directions of our NO_2 trends are consistent with previous studies that have focused on large cities around the world (*25*, *27*, *33*–*35*). This consistency includes trend reversals from positive to negative over Jakarta and Riyadh in 2011 and from negative to positive over Manila in 2009 (*34*, *35*). The significant increases in NO_2 in Northwest African cities, ranging from 2.0% a^{-1} over N'Djamena to 4.4% a^{-1} over Niamey and Lagos, are opposite to the large regional decline in NO_2 of 4.5% a^{-1} reported by Hickman *et al.* (*16*) for the same instrument used here. These authors focused on the dry season (November to February) when intense and widespread open burning of biomass is prevalent.

As with NO_2, NH_3 increases in almost all tropical cities in Africa, the Middle East, and Southeast Asia (Fig. 2B). Known dominant sources include agricultural activity, vehicles, and burning of waste and biomass in all regions, as well as large-scale industrial fertilizer production in Asia (*36*, *37*). The increase in NH_3 over Jakarta while NO_2 declines could reflect absence of air quality policies targeting agriculture and biomass burning (*26*). Decline in NH_3 in almost all South Asian cities coincides with increases in precursor (SO_2) emissions of acidic sulfate aerosols (*38*, *39*) that promote partitioning of

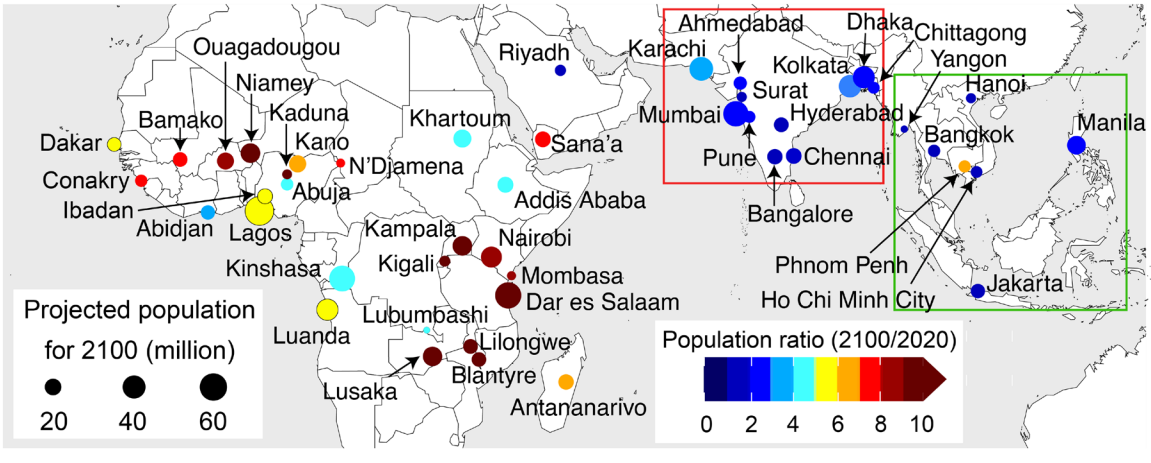

Fig. 1. Projected population growth for the fastest-growing cities in the tropics (25°S to 25°N) anticipated to be megacities (population ≥ 10 million) by 2100. Circle sizes indicate the projected 2100 population, and colors are 2100-to-2020 population ratios as indicators of population growth. Data for 2100 are from Hoornweg and Pope (*2*) and, for 2020, from the United Nations (UN) (*1*). Boxes discern cities in South Asia (red) and Southeast Asia (green).

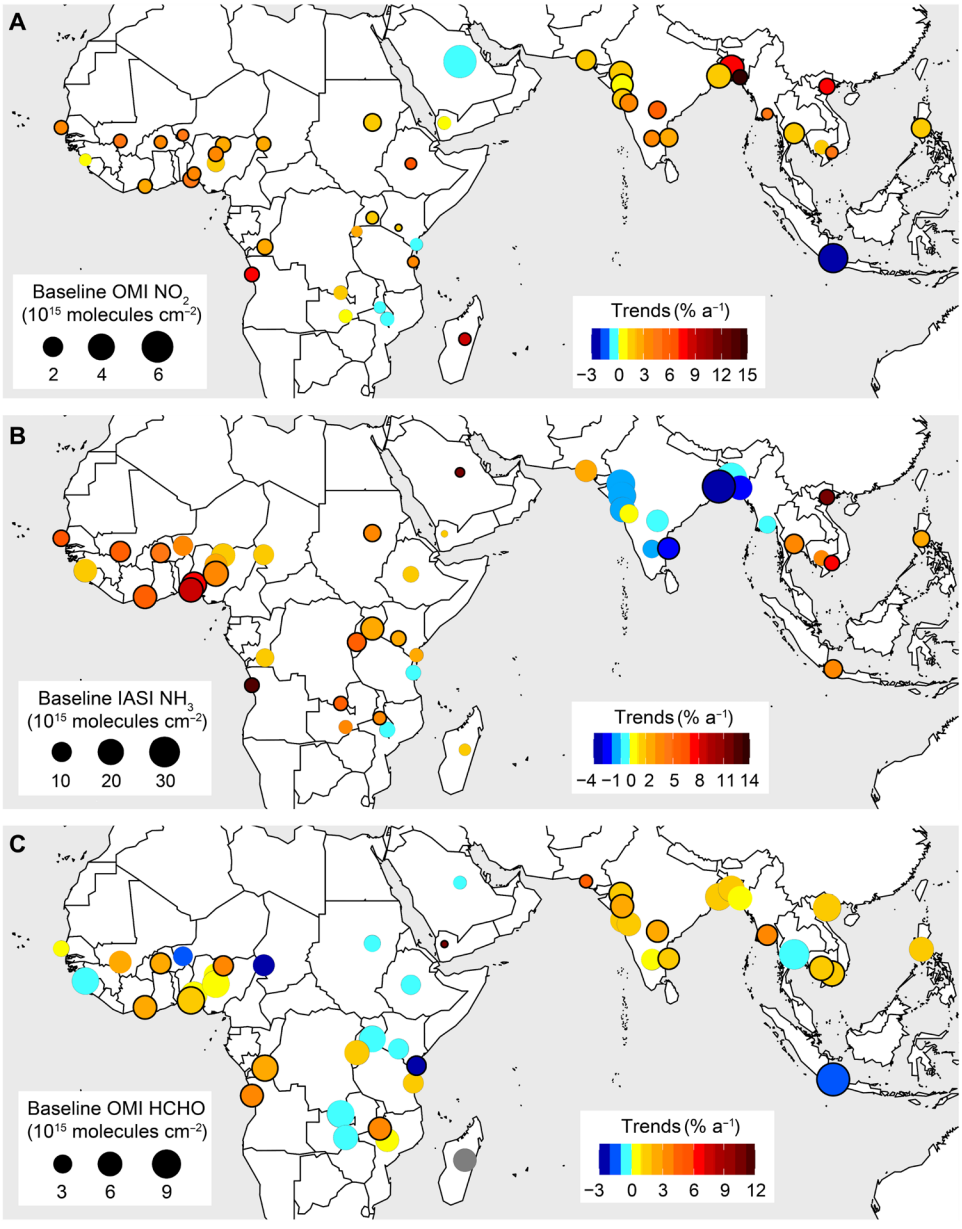

Fig. 2. Trends in NO_2, NH_3, and reactive NMVOCs in rapidly growing cities in the tropics. (**A** to **C**) Trends in NO_2 and reactive NMVOCs are for 2005–2018 and in NH_3 for 2008–2018. Circle colors are the relative trends, and sizes are values at the start of the record (baseline). Outlines identify significant trends at the 95% confidence interval (CI). Warm colors indicate positive trends, and cool colors indicate negative trends. The trend in reactive NMVOCs at Antananarivo in Madagascar is gray because of the low temporal coverage. Trend values are in table S1. OMI, Ozone Monitoring Instrument; IASI, Infrared Atmospheric Sounding Interferometer.

NH_3 to acidic aerosols to form $PM_{2.5}$ (*40*). In India, SO_2 emissions, mostly from industry and coal-fired power plants, are estimated to have increased by 50% from 2007 to 2016 (*41*). Aerosol partitioning of NH_3 would also be promoted by an increase in abundance of acidic nitrate aerosol due to an increase in precursor emissions of NO_x, supported by our positive trends in NO_2 (Fig. 2A). Increase in abundance of chlorine from plastic waste fires would also promote aerosol uptake of NH_3 (*42*), but there are no routine measurements to quantify trends in chlorine abundance. Increases in waste generation and absence of effective waste management support an increase in chlorine emissions from this source (*43*). Karachi is the lone city in South Asia with an increase in NH_3 of 2.9% a^{-1}. This may reflect increased use of synthetic fertilizers and excess NH_3 from intense agricultural fires across the Indo-Gangetic Plain (*6*, *26*, *44*), although this increase is not significant. NH_3 column densities at the start of the record are similar for Asia and Africa, due to a combination of similar sources (*36*, *37*, *44*). Our positive city trends are generally 1.5 to 2.5 times steeper than the trends at regional and national scales reported by Van Damme *et al.* (*26*). The steeper trends in cities could be due to greater abundance of urban sources of NH_3 (*36*, *45*) and enhanced NH_3 volatilization due to the urban heat island effect (*46*).

Table 1. Satellite data products used to determine trends in NO_2, reactive NMVOCs, NH_3, and AOD for fast-growing cities in the tropics.

Instrument	Launch platform	Launch date	Swath width	Measurement	Product name	Pixel resolution	Overpass time	Global coverage	Data retained
OMI*	Aura	October 2004	2600 km	NO_2	NASA SP v4.0†	13 km by 24 km‡	13 h30 LST§	Every 2 days‖,¶	Cloud fraction < 50% Terrain reflectivity < 30% Solar zenith angle < 85° Processing error flag = 0 Processing quality flag = 0 Cloud fraction < 50%
				HCHO	QA4ECV v1.3#				
IASI**	Metop-A	October 2006	2130 km	NH_3	v3R††	12 km‡,‡‡	09 h30 LST§	Daily‖	Cloud fraction < 10%
MODIS§§	Aqua	May 2002	2230 km	AOD	Merged SDS C6.1‖‖	10 km by 10 km‡	13 h30 LST§	Near-daily‖	Quality assurance flag = 3

*Ozone Monitoring Instrument. †NASA Standard Product version 4.0 (https://doi.org/10.5067/Aura/OMI/DATA2017; last accessed 18 March 2021). ‡At nadir. §Local solar time. ‖Time to achieve global coverage for relevant satellite overpass time. ¶Global coverage degraded from daily in 2005–2009 to every 2 days thereafter due to the row anomaly. #Quality Assurance for Essential Climate Variables version 1.3 (https://doi.org/10.18758/71021031; last accessed 18 March 2021). **Infrared Atmospheric Sounding Interferometer. ††Reanalyzed IASI version 3.0.0 (https://iasi.aeris-data.fr/NH3R-ERA5_IASI_A_data/; last accessed 20 March 2021). ‡‡Circular pixels at nadir. §§Moderate Resolution Imaging Spectroradiometer. ‖‖Merged Scientific Data Set Collection 6.1 (https://doi.org/10.5067/MODIS/MYD04_L2.061; last accessed 18 March 2021).

Trends in HCHO as a proxy for reactive NMVOCs (Fig. 2C) are not as homogeneous or significant as trends in NO_2 and NH_3, apart from Jakarta and cities in South Asia. Significant decline in reactive NMVOCs in Jakarta of 1.7% a^{-1} is similar to that for NO_2 (Fig. 2A). This could be due to a decrease in vehicle exhaust emissions of unburned reactive hydrocarbons from enhanced efficiency of diesel vehicles due to greater use of biodiesel (*47*). Biodiesel usage in Indonesia has increased 16-fold from 2010 to 2019 (*48*). Our upward trends in reactive NMVOCs for Lagos (1.5% a^{-1}), Mumbai (1.7% a^{-1}), and Kinshasa (2.0% a^{-1}) support sustained increases in reactive NMVOCs identified for 1997–2009 using an earlier record of satellite observations (*29*). The trend for Mumbai is not significant. The greatest increase in reactive NMVOCs occurs over Sana'a (>10% a^{-1}), although the HCHO column densities there are close to the instrument detection limit and very small (<1 × 10^{15} molecules cm^{-2}) at the beginning of the record after removing the background contribution (Materials and Methods). The population in Sana'a has increased by 4.7% a^{-1}, but the country has also been embroiled in conflict and political instability, and the increase in the other pollutants is marginal (0.07 to 1.15% a^{-1}) (table S1).

In nine African cities (Conakry, Niamey, N'Djamena, Addis Ababa, Nairobi, Kampala, Khartoum, Lubumbashi, and Lusaka), reactive NMVOCs decline at the same time as NO_2 increases, consistent with a shift to more efficient combustion sources, as is suggested by regional anthropogenic emission inventories (*10*, *12*). Rates of increase in reactive NMVOCs in cities in South Asia of 0.6 to 4.3% a^{-1} are less steep than trends in NO_2 (0.8 to 14.1% a^{-1}). The generally positive, steeper, and greater number of significant trends in NO_2 (and thus NO_x) compared to those of reactive NMVOCs has implications for surface ozone formed from photochemical oxidation of NMVOCs in the presence of NO_x. In most of the tropics, surface ozone is near the WHO 8-hour mean guideline of 100 μg m^{-3} (*49*) and, at these levels, is harmful to staple crops prevalent there (*50*). Ratios of total column HCHO (background + reactive NMVOCs) to tropospheric column NO_2 (HCHO/NO_2; fig. S4) in 2005 exceed values of 2 in almost all cities (reaching 23 in Conakry and Nairobi), indicative of chemical regimes in which ozone formation is sensitive to NO_x sources. During the record of NO_2 and HCHO observations used here (2005–2018), most of these cities are transitioning to a regime in which ozone production is sensitive to NMVOC sources, synonymous with many megacities in the United States, Europe, and China. If the future mimics the past, then the transition to sensitivity to NMVOCs could occur as soon as 2025 in Chittagong and Dhaka and 2030 in Addis Ababa, Hanoi, and Luanda. As NMVOCs are especially challenging to monitor and regulate (*6*, *51*), these trends suggest that there should be swift implementation of policies targeting NO_x sources to halt the transition to a VOC-sensitive ozone production regime.

Figure 3 shows trends in AOD, which we interpret as trends in surface concentrations of $PM_{2.5}$ (*6*). The relationship between AOD and $PM_{2.5}$ is complicated by $PM_{2.5}$ composition, vertical distribution of aerosols, relative humidity, cloud cover, and seasonality in planetary boundary layer dynamics and synoptic-scale meteorology (*52*–*55*). This causes inconsistencies in month-to-month variability in AOD and surface concentrations of $PM_{2.5}$ but not in the long-term trends (*6*). AOD at the start of the record is >0.25 over cities in West Africa, the Middle East, South Asia, and Southeast Asia due to a mix of large aerosol sources such as biomass burning and vehicular emissions in all these regions; desert dust in West Africa, the Middle East, and South Asia; and large industrial sources in Asia (*56*–*58*).

Trends in AOD from 2005 to 2018 in South Asian cities are steep (2.5 to 7.8% a^{-1}) and significant. AOD more than doubles in

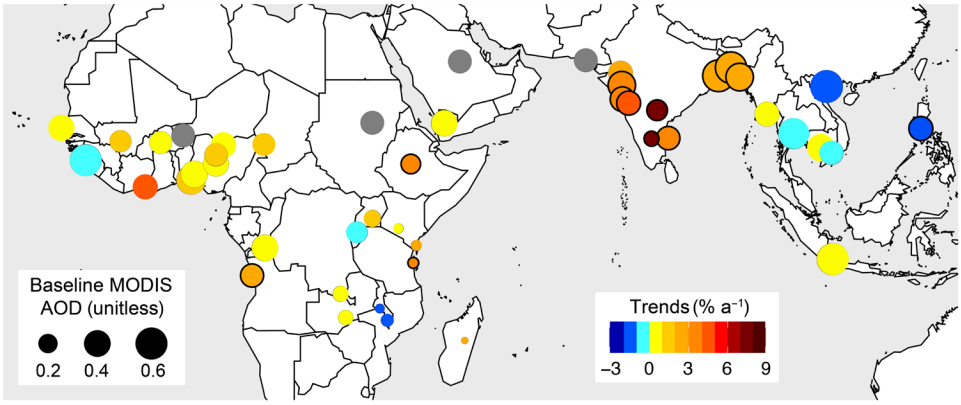

Fig. 3. Trends in AOD as proxy for $PM_{2.5}$ abundance in rapidly growing cities in the tropics for 2005–2018. Circle colors are relative trends in AOD, and sizes are values at the start of the record (baseline). Outlines identify significant trends at the 95% CI. Warm colors indicate positive trends, and cool colors indicate negative trends. Cities with poor temporal coverage are gray. AOD trend values are in table S1. MODIS, Moderate Resolution Imaging Spectroradiometer.

Bangalore (7.8% a^{-1}) and Hyderabad (7.3% a^{-1}). Earlier studies have reported similar positive trends for these cities (*28*, *39*), so our contemporary record supports sustained rapid growth in AOD (and thus $PM_{2.5}$). Desert dust likely does not contribute to trends in AOD over South Asian cities, as desert dust optical depth has declined over the Thar Desert and makes a negligible contribution to AOD trends across the rest of India (*59*). This suggests that the substantial increase in $PM_{2.5}$ in South Asia is due to increased formation of secondary inorganic aerosols resulting from increases in SO_2 emissions forming aerosol sulfate (*38*, *39*), NO_x emissions forming aerosol nitrate (Figs. 2A and 4G), and buffering by ammonium formed when NH_3 partitions to these acidic aerosols, which leads to declining NH_3 abundance (Fig. 2B). The increase in reactive NMVOCs (Fig. 2C), which includes precursors of secondary organic aerosols, likely also contributes to the increase in $PM_{2.5}$.

Trends in cities in other regions are not as consistent as for South Asia. In Southeast Asia, only Manila shows a significant decline in $PM_{2.5}$ (−2.0% a^{-1}), while, in Africa, there are significant increases in Luanda (2.3% a^{-1}), Addis Ababa (3.3% a^{-1}), and Dar es Salaam (3.3% a^{-1}). The significant increase in AOD for Addis Ababa may be influenced by the positive trend in desert dust optical depth over Ethiopia (*59*). $PM_{2.5}$ increases in Jakarta despite a significant decrease in precursor emissions of NO_x (Fig. 2A) and reactive NMVOCs (Fig. 2C). This may be due to an increase in sulfate in Jakarta from high sulfur fuel combustion and regional adoption of coal-fired power generation (*60*, *61*) as well as lack of policies targeting biomass burning and agricultural sources. Our positive trends in AOD for most West African cities are opposite to the reported weak regional decline in AOD of 0.1% a^{-1} (*62*).

Disentangling underlying sources influencing trends in air quality

To assess whether conventional biomass burning or emerging anthropogenic sources dominate tropical city trends in air quality, we separate the satellite data into biomass burning and nonbiomass burning data, compare trends in these categories to trends in all the data (Fig. 2), and confirm that the nonbiomass burning data are dominated by anthropogenic activity for pollutants that also have large natural sources. The trend comparison is shown in Fig. 4 for the 22 tropical cities that we identify to be substantially influenced by biomass burning (Materials and Methods). In general, there are fewer significant trends in biomass burning (Fig. 4, A to C) than there are in anthropogenic activity (Fig. 4, D to F). The Fig. 2 trends in the reactive NMVOC portion of the HCHO column appear to be predominantly influenced by anthropogenic activity. This is supported by either the same or steeper trends in anthropogenic activity data than all data (Fig. 4F), by lack of consistent trends for all but one city in the biomass burning comparison (Fig. 4C), and by absence of significant trends in biogenic VOCs determined by sampling HCHO in surrounding rural areas that should be dominated by biogenic VOCs (in particular isoprene) (Supplementary Text).

Anthropogenic activity appears to be the driving force for trends in NO_2 in most cities (Fig. 4D), although some cities have similar positive trends in biomass burning and all data (shapes along the 1:1 line in Fig. 4A). Six African cities exhibit very steep increases in anthropogenic activity NO_2 of 1.6 to 9.8% a^{-1} (points above the gray shading in Fig. 4D). Three of these, all in West Africa (Abuja, Ibadan, and Conakry), lie below the gray shading in Fig. 4A, suggesting that negative or muted trends in biomass burning dampen the effect of increasing anthropogenic activity on degradation in air quality. This is consistent with findings from the regional study by Hickman *et al.* (*16*) and supported by a decline in burned fraction for the two cities in Nigeria (Abuja and Ibadan; fig. S3). Regional bottom-up inventories also suggest that anthropogenic emissions already or will soon rival those from biomass burning (*10*, *12*).

The NH_3 trends (Fig. 4, B and E) exhibit a compensating effect between anthropogenic activity and biomass burning in many cities. Six cities with steep increases in anthropogenic activity of 1.0 to 31.6% a^{-1} have negative trends in biomass burning, and three West African cities (Lagos, Kaduna, and Abidjan) with steep increases in biomass burning have much shallower trends in anthropogenic activity. These same three cities exhibit positive trends in burned fraction but not in biomass burning NO_2 (Fig. 4A) or reactive NMVOCs (Fig. 4C). This may be due to a shift in the type of vegetation burned (*63*), a transition to more anoxic fires favoring NH_3 over NO_x and longer-lived hydrocarbons over reactive oxygenated VOCs, or due to greater prevalence in the dry season of anthropogenic NH_3 sources such as waste burning. Evidence of these shifts requires further investigation.

We also assess the skill of a contemporary anthropogenic emission inventory at reproducing trends in Fig. 2 for all 46 cities

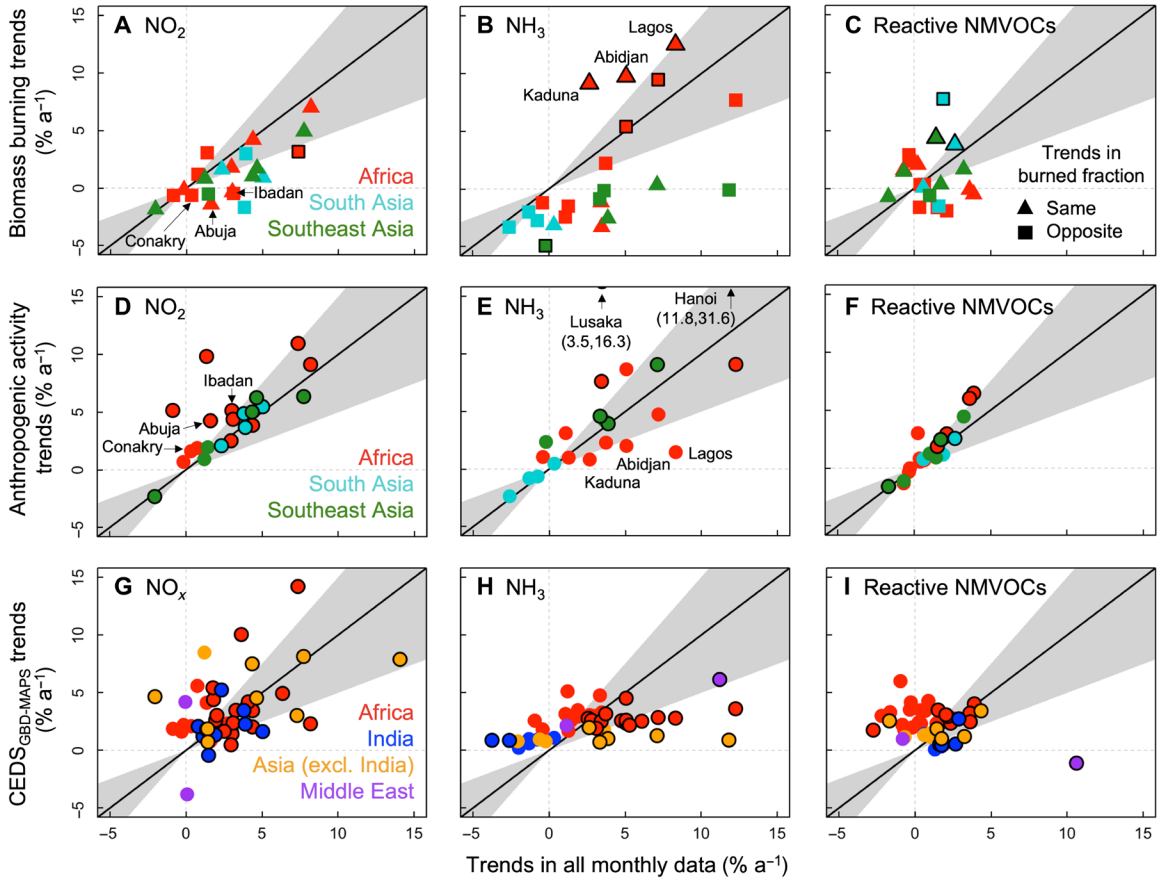

Fig. 4. Constraints on factors influencing trends in short-lived air pollutants in rapidly growing cities in the tropics. Panels compare trends in all data (Fig. 2) to trends in biomass burning (**A** to **C**) and anthropogenic activity (**D** to **F**) for 22 cities influenced by biomass burning (fig. S3 and Materials and Methods) and to trends in bottom-up anthropogenic emissions (**G** to **I**) for all 46 cities. Shape colors distinguish regions, and, in (A) to (C), shape types indicate trends that are consistent with (triangles) or opposite to (squares) the trends in burned fraction (fig. S3). Outlines identify significant trends at the 95% CI for biomass burning (A to C), anthropogenic activity (D to F), and all data (G to I). Trends are significant for Lusaka and Hanoi in (E), which are off scale. The gray shading is the ±50% spread around the black 1:1 line. Dotted lines discern positive and negative trends.

(Fig. 4, G to I), as satellite observations provide constraints on precursor emissions of short-lived pollutants (*25*, *30*, *37*) and because we find that anthropogenic activity dominates trends in air quality in tropical cities. We use the global contemporary $CEDS_{GBD\text{-}MAPS}$ inventory (Materials and Methods) that has been applied in the Global Burden of Disease (GBD) studies (*64*). $CEDS_{GBD\text{-}MAPS}$ NO_x emission trends reproduce the direction of trends in satellite NO_2 for most cities (Fig. 4G), although, for many, the discrepancy exceeds 50%. $CEDS_{GBD\text{-}MAPS}$ does not capture the policy-driven decline in emissions in Jakarta (+4.7% a^{-1} in $CEDS_{GBD\text{-}MAPS}$ and −2.0% a^{-1} in the observations) or the marginal, although nonsignificant, increase in NO_x in Sana'a (−3.8% a^{-1} in $CEDS_{GBD\text{-}MAPS}$ and +0.07% a^{-1} in the observations). According to $CEDS_{GBD\text{-}MAPS}$, the steepest increases in NO_x emissions in African cities are from nonresidential energy generation (4.6% a^{-1}) and industry (4.2% a^{-1}). These sources together account for 65 to 70% of $CEDS_{GBD\text{-}MAPS}$ NO_x in Indian cities, but the steepest increases are for off-road transport (8.6% a^{-1}) and a mix of nontraditional combustion sources (2.8% a^{-1}). In Asian cities, excluding India, the largest growth in $CEDS_{GBD\text{-}MAPS}$ NO_x is from the dominant sectors' energy generation (4.2% a^{-1}), industry (5.3% a^{-1}), and off-road transport (6.3% a^{-1}).

Changes in NO_x lifetime and the relative contribution of the free tropospheric portion of the column may also contribute to divergence in column and emission trends. Most studies assessing these effects have focused on cities in the northern hemisphere that have experienced substantial policy-driven decline in NO_x emissions (*65*, *66*). Results from these studies suggest that NO_x lifetime and background changes as NO_x emissions increase in VOC-rich environments typical of the tropics (fig. S4) should have opposing effects on agreement between trends in NO_2 columns and NO_x emissions. Trends in the column are likely steeper than trends in emissions because of decline in NO_x lifetime, whereas trends in the NO_2 column should be dampened relative to trends in emissions because of decline in the relative contribution of the NO_x background.

Trends in $CEDS_{GBD\text{-}MAPS}$ NH_3 emissions are positive for all cities, but two to five times less than the observed trends (Fig. 4H). Underestimates in $CEDS_{GBD\text{-}MAPS}$ trends are greatest for all but two of the cities that we identified to be strongly influenced by steep increases in anthropogenic sources (Fig. 4E). Similarly large underestimates in emission inventory trends have been reported at the regional and national scale (*26*). Inventories may underestimate rapid changes in agricultural activity, such as increases in livestock numbers and adoption of synthetic nitrogen fertilizers (*67*, *68*). Growth in agricultural productivity in sub-Saharan Africa is almost

double the global average (*68*). Waste burning is another prevalent source of NH_3. Waste generation is projected to increase by 2 to 6% a^{-1} across the tropics over the next three decades (*69*). Much of this will be burned if ineffective waste management persists. Divergence of NH_3 trends in Indian cities and nearby Asian cities is due to the increase in acidic aerosols already discussed. According to $CEDS_{GBD\text{-}MAPS}$, NH_3 emissions in Indian cities grew at a rate of 1% a^{-1}, mostly due to a 2% a^{-1} increase in agricultural emissions. Discrepancies in observed and $CEDS_{GBD\text{-}MAPS}$ NH_3 in Riyadh and Sana'a are large, but emissions for these cities are small [3 to 10 kilotons (kt) a^{-1} during 2005–2017] compared to the other tropical cities (30 to 80 kt a^{-1} for the same time period) and mainly come from waste processing.

Trends in bottom-up and top-down reactive NMVOCs are generally similar for cities with significant increases in these and are dominated by increases in residential energy combustion in $CEDS_{GBD\text{-}MAPS}$. Trends diverge for Sana'a (−1.1% a^{-1} for $CEDS_{GBD\text{-}MAPS}$ and +10.6% a^{-1} for the observations), but observed values are small and may be prone to error. As with NO_2, $CEDS_{GBD\text{-}MAPS}$ trends in reactive NMVOCs in Jakarta (+2.6% a^{-1}) are opposite to the observations (−1.7% a^{-1}). Significant decline in reactive NMVOCs over Mombasa in the observations (−2.7% a^{-1}), but not in the inventory (+1.8% a^{-1}), may be due to a shift toward combustion-efficient sources due to substantial development of the Mombasa seaport to meet increasing demand for imported goods (*70*), although this is not supported by the nonsignificant decline in NO_2 (0.3% a^{-1}; Fig. 2A).

Increase in premature deaths from enhanced exposure to air pollutants hazardous to health

Urban population in the tropical cities in Fig. 1 increased on average by 2 to 10% a^{-1} in Africa, 4 to 5% a^{-1} in the Middle East, 1 to 7% a^{-1} in South Asia, and 1 to 8% a^{-1} in Southeast Asia from 2005 to 2018. Rapid population growth combined with steep and significant increases in NO_2 in most cities (Fig. 2A) and in $PM_{2.5}$ in all cities in South Asia and many in Africa (Fig. 3) will substantially increase population exposure to hazardous pollutants. The effects of long-term exposure to ambient air pollution includes well-established health outcomes such as respiratory and cardiovascular diseases (*71*, *72*) and recently identified health end points such as dementia, impaired cognition, and loss of fertility and eyesight (*73*–*77*). Premature mortality due to exposure to ambient $PM_{2.5}$ from anthropogenic sources is already substantial in Asia but is relatively low in Africa, particularly in comparison to communicable diseases and exposure to indoor air pollution and ambient pollution from natural sources (*19*, *20*, *64*, *71*). Hickman *et al.* (*16*) suggest, using the same NO_2 observations, that regional air quality in Africa has improved because of decline in biomass burning activity. Their analysis, however, focused on the burning season and did not account for rapid growth in urban population, enhancing population exposure to air pollution.

The trends in exposure to $PM_{2.5}$ and NO_2 that we obtain for the 46 tropical cities (Materials and Methods) are shown in Fig. 5. Population exposure to $PM_{2.5}$ increases in all cities except Manila (−0.8% a^{-1}), where a 2.0% a^{-1} decline in $PM_{2.5}$ (Fig. 3) counters an equivalent increase in population. Exposure to NO_2 increases in all cities except Jakarta (−1.2% a^{-1}), although the absolute health gains due to decline in exposure to NO_2 in Jakarta will be more than offset by a 1.8% a^{-1} increase in exposure to $PM_{2.5}$ due to a 1.3% a^{-1} increase in population and a small, although not significant, increase in $PM_{2.5}$ (0.5% a^{-1}; Fig. 3). In general, upward trends in exposure are 1.5 to 3.0 times steeper than the positive trends in $PM_{2.5}$ (Fig. 3) and NO_2 (Fig. 2A) alone. Increases in population exposure to $PM_{2.5}$ are 3.1 to 17.9% a^{-1} in South Asian cities and >10% a^{-1} in Addis Ababa (10.6% a^{-1}), Abuja (10.7% a^{-1}), Antananarivo (13.0% a^{-1}), Luanda (11.7% a^{-1}), and Dar es Salaam (14.8% a^{-1}) in Africa. These same African cities also experience the steepest increases in NO_2 exposure of >12% a^{-1}. Across Africa, the increase in exposure to NO_2 ranges from 2.0% a^{-1} in Blantyre to 21.3% a^{-1} in Luanda and 23.0% a^{-1} in Antananarivo.

Figure 6 ranks the 15 cities with the largest increases in the number of premature deaths over the 14-year observing period, mostly in Asia (13 of 15). Premature deaths range from 3500 in Lagos to 24,000 in Dhaka. Values for each city are in table S2. These are obtained by calculating absolute $PM_{2.5}$ in each city using our annual trends in AOD (Fig. 3) and $PM_{2.5}$ from a chemical transport model for a single year at the center of the observing period (2012) and applying these to a health risk assessment model that relates the risk of premature mortality to ambient $PM_{2.5}$ (Materials and Methods). We focus on $PM_{2.5}$ because of its much greater health risk than NO_2 (*78*, *79*). Increased incidence of morbidity will also result from the substantial increases in population exposure to $PM_{2.5}$ and NO_2 (Fig. 5). The increase in premature mortality, summed over the cities in Fig. 1 with discernible trends in AOD (Fig. 3), is 180,000 [95% confidence interval (CI): −230,000 to 590,000], an average increase of 13,000 each year. This is a 62% increase in premature deaths due to $PM_{2.5}$ exposure, from 290,000 (95% CI: 200,000 to 370,000) in 2005 to 470,000 (95% CI: 70,000 to 870,000) in 2018. The contribution to total premature deaths increases from 27% in 2005 to 32% in 2018, and the number of cities where at least one-third of deaths is attributable to exposure to $PM_{2.5}$ increases from 14 in 2005 to 20 in 2018. $PM_{2.5}$ exposure persists as the leading cause (>50%) of premature deaths in Kano (Nigeria), N'Djamena (Chad), and Kolkata (India).

Premature mortality estimates for 2005 and for 2008 are significant for almost all cities (table S2). The wide range in the premature mortality 95% CIs is due to large uncertainty in the health risk assessment model for annual mean $PM_{2.5} > 50$ μg m^{-3} (*19*, *79*), typical of most cities in South Asia and West Africa. As the 95% CIs for 2005 and 2018 overlap, changes in premature mortality are not significant for most cities (as indicated in table S2) and in the total given in Fig. 6. Kolkata makes the largest contribution to uncertainties in the total, as $PM_{2.5}$ there is much greater than 50 μg m^{-3}, increasing from 78.8 μg m^{-3} in 2005 to 106.3 μg m^{-3} in 2018 (table S2). The total increase in premature deaths from 2005 to 2018 without Kolkata is 165,000, and the lower limit of the CI exceeds zero (95% CI: 40,000 to 290,000).

We also determine the contribution of individual factors ($PM_{2.5}$, population, and baseline mortality) to changes in total premature mortality (Materials and Methods, fig. S5, and table S3). African cities experience substantial decline in baseline mortality that reduces the impact of increases in population and $PM_{2.5}$ on premature mortality. Decline in baseline mortality more than offsets increases in the other factors in Blantyre, Lilongwe, and Kaduna, leading to decline in premature mortality attributable to $PM_{2.5}$. The significant 3.1% a^{-1} increase in NO_2 in Kaduna may still lead to severe public health outcomes. The increase in premature mortality in South Asian cities is due exclusively to population and $PM_{2.5}$. Although trends in

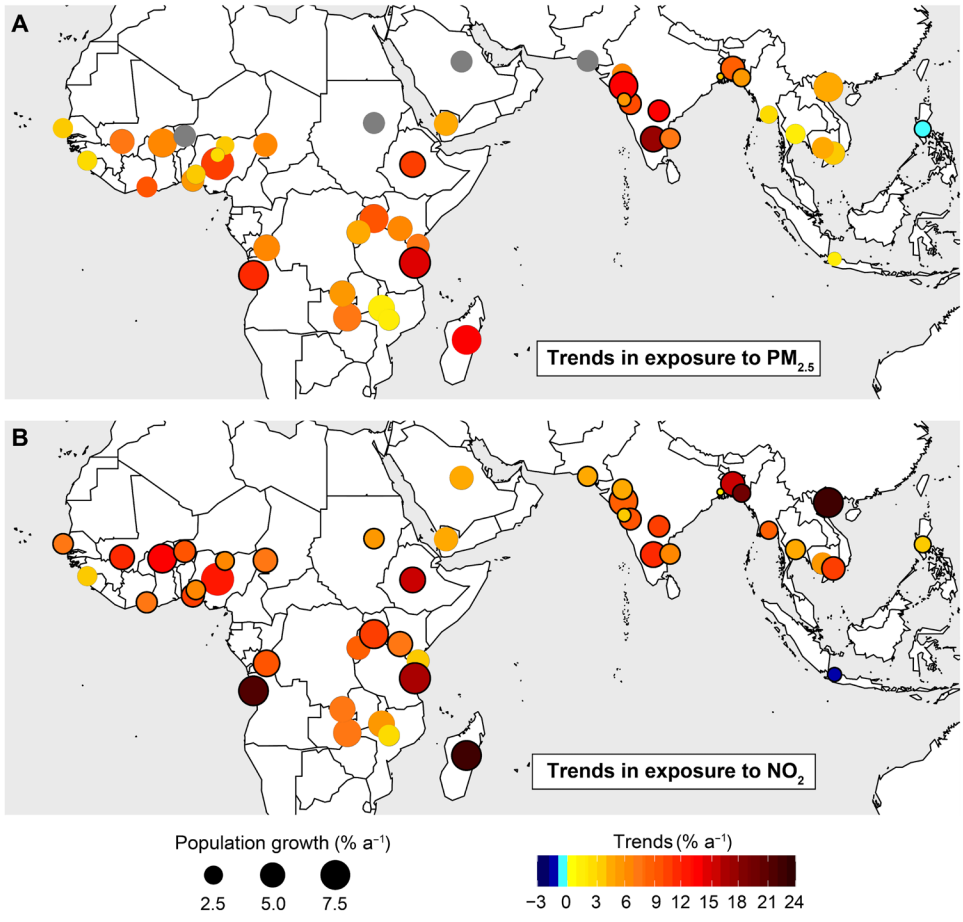

Fig. 5. Trends in exposure to air pollutants hazardous to health in rapidly growing tropical cities. Circle colors are trends in exposure to $PM_{2.5}$ (**A**) and NO_2 (**B**). Circle sizes are annual average increases in urban population from 2005 to 2018. Outlines identify cities with significant trends in $PM_{2.5}$ (Fig. 3) and NO_2 (Fig. 2A) at the 95% CI. Cities with low temporal coverage in AOD are gray.

premature mortality are positive for all Southeast Asian cities, the relative contribution of each factor is mixed. The contribution of factors in Phnom Penh and Yangon is similar to African cities. Decline in $PM_{2.5}$ in Bangkok, Hanoi, Ho Chi Minh City, and Manila does not mitigate the influence of increases in population and baseline mortality.

Our premature mortality estimates for 2005 and 2018 are on median a factor of 3 more than those reported for the same cities in studies that determine premature mortality using the Integrated Exposure-Response (IER) model that is also applied to GBD studies (*80*–*83*). The IER model uses health data from active smoking, secondhand tobacco smoke, and indoor air pollution to derive a relationship between outdoor $PM_{2.5}$ exposure and risk of premature mortality. Updated health risk assessment models that no longer rely on proxies for ambient $PM_{2.5}$ and incorporate data from global cohort studies, such as the Global Exposure Mortality Model (GEMM), yield premature mortality estimates that are more than double those from the GBD (*71*). We use an updated health risk assessment model (*79*) that is derived with more cohort studies and health end points covering a wider age range (14 years and older) and $PM_{2.5}$ concentration range than both the IER model and the GEMM (*71*, *83*). In our previous work, we showed that this new health risk assessment model yields premature mortality estimates that are 50% more than those estimated with the GEMM (*19*). The GEOS-Chem model version that we use typically overestimates surface $PM_{2.5}$ by 5 to 10% estimated from comparison to surface observations for North America and Europe and satellite-derived $PM_{2.5}$ for Africa (*19*, *84*). If we artificially decrease modeled $PM_{2.5}$ by 10%, then we find that the additional premature mortality from 2005 to 2018 only changes by 6%. Decreasing from 180,000 deaths to 170,000.

DISCUSSION

With our targeted sampling of satellite observations over 46 densely populated fast-growing tropical cities, we find large and significant increases in NO_2, NH_3, reactive VOCs, and AOD (and thus $PM_{2.5}$) in these cities at rates two to three times faster than or opposite in sign to national and regional trends. The degradation in air quality in the past two decades is mostly influenced by anthropogenic activity rather than traditional widespread open burning of biomass. Only Jakarta shows evidence of air quality improvements due to policy measures, and those improvements have had a limited effect, leading to decline in NO_2 and reactive VOCs but not in NH_3 or $PM_{2.5}$.

We also determine that ozone formation is on track to transition from strongly NO_x-sensitive to the more challenging to regulate

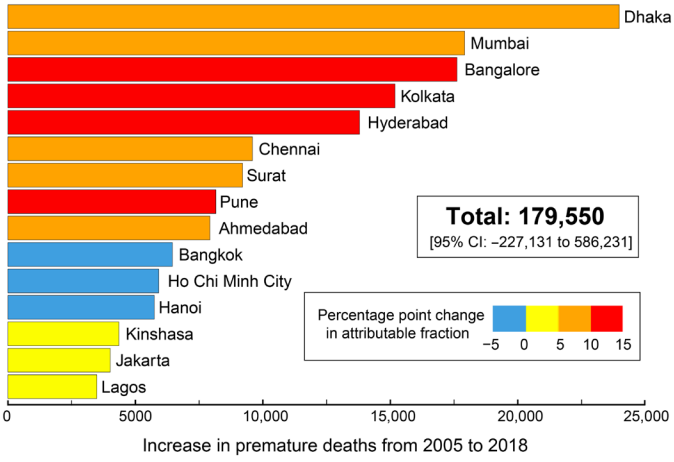

Fig. 6. Increase in premature deaths due to increase in exposure to $PM_{2.5}$ in rapidly growing tropical cities. Bars give the increase in premature mortality in 2018 relative to 2005 for the top 15 tropical cities, colored by the percentage point change in fraction of premature deaths attributable to exposure to $PM_{2.5}$. Inset value is the total for the cities in Fig. 1 with detectable trends in AOD (Fig. 3). Values for all cities are in table S2, and the relative contribution of individual factors ($PM_{2.5}$, population, and baseline mortality) is in fig. S5.

VOC-sensitive regime. In some cities, this may occur as early as 2025. We find large increases in population exposure to hazardous air pollutants $PM_{2.5}$ and NO_2 and estimate 13,000 additional premature deaths each year from this increase in population exposure to air pollution. These trends will almost certainly be sustained in the future because of projected population growth (Fig. 1) and absent effective air quality policies.

The predicted population for 2100 predates the coronavirus disease 2019 (COVID-19) pandemic, but unemployment, inequitable health care access, and reduced fertility resulting from the pandemic (*85*, *86*) are only likely to delay rather than prevent the deleterious effects of exposure to air pollution that our findings suggest. The pandemic has demonstrated that health care systems in tropical countries are vulnerable to the looming health crisis supported by our exposure trends. Immediate and strict policy measures are needed to improve air quality and curtail increased exposure to hazardous pollutants due to abrupt population growth and urbanization in a part of the world that accounts for an increasingly large portion of the global population.

MATERIALS AND METHODS

Satellite datasets, city sampling, and trend estimates

We use Earth observations of tropospheric column NO_2 and total column HCHO from the Ozone Monitoring Instrument (OMI), attenuation of light by aerosols throughout the atmospheric column or AOD from the Moderate Resolution Imaging Spectroradiometer (MODIS), and total column NH_3 from the Infrared Atmospheric Sounding Interferometer (IASI) to determine trends in air quality, precursor emissions, and population exposures over the rapidly growing tropical cities identified in Fig. 1. The record of observations we use is for 2005–2018 from OMI and MODIS and for 2008–2018 from IASI. Table 1 provides additional details of the instrument features, satellite data products, and data quality flags used to process the data. In our previous work, we demonstrated that these space-based observations of tropospheric column NO_2 and total column NH_3 reproduce month-to-month variability in surface concentrations of these and that satellite observations of AOD reproduce long-term trends in surface observations of $PM_{2.5}$ (*6*). The same assessment of the skill of satellite observations of HCHO in reproducing changes in surface concentrations of reactive NMVOCs was not possible, as measurements of reactive NMVOCs are sparse in space and time and routine measurements are limited to hydrocarbons.

We calculate city-wide monthly means by sampling satellite pixel centers that fall within the city boundaries using shapefiles mostly from the Database of Global Administrative Areas (GADM) version 3.6 (https://gadm.org/; last accessed 12 March 2021). Satellite data coverage can be low for smaller cities, exacerbated by persistent clouds in the tropics. We address this by extending the sampling domain beyond the city boundaries relative to the instrument pixel size (6.5 km for OMI and MODIS and 10 km for IASI), as in (*6*), for the 22 smallest tropical cities (indicated in table S1). In our analysis, we only retain months with at least 5 pixels, as in (*6*).

We isolate the contribution of local HCHO sources (direct emissions and oxidation of reactive NMVOCs) to total column HCHO by subtracting the background column component due to oxidation of methane and other long-lived VOCs (*6*, *30*). We do this by calculating monthly mean background columns over remote ocean domains closest to the cities of interest that extend over the same latitudinal range as the selected cities (fig. S2), where feasible. This ensures consistent seasonality between the background column and columns over the target cities. We then apply the nonlinear fit described in (*87*) that accounts for seasonality in the time series to the monthly mean background HCHO and subtract the fitted values from the city-wide monthly means, as in (*30*) and (*6*). We also assess the contribution of biogenic VOCs to trends in reactive NMVOCs by sampling HCHO over a 0.2° by 0.2° rural area 50 to 100 km away from the city.

All atmospheric components of interest in this work exhibit a distinct seasonality in the tropics due to seasonality in photochemistry, planetary boundary layer dynamics, synoptic meteorological events such as monsoons, and sources such as biomass burning (*6*, *26*, *88*). To account for this in the trend analysis, we fit the nonlinear function from van der A *et al.* (*87*) to the time series of city-wide monthly means. This is only applied to cities with >30% temporal coverage (>50 months for OMI and MODIS and >40 months for IASI). Cities with too few monthly means are shown as gray circles in Figs. 2 and 3, and fig. S4. Trends are considered significant at the 95% CI ($P < 0.05$) if the CI range does not intersect zero.

Trends in biomass burning and anthropogenic activity

Intense regional open burning of biomass contributes to large seasonal enhancements in air pollution in the tropics, and anthropogenic activity dominates the nonbiomass burning period (*7*, *9*, *89*). To determine whether biomass burning or anthropogenic activity influences trends in NO_2, NH_3, and reactive NMVOCs (Fig. 2), we separate city-wide monthly means into months above and below the 75th percentile in each year. We find that months above 75th percentile values coincide with months known to be influenced by biomass burning in 22 of the cities in Fig. 1 (indicated in fig. S3). These are December to March in Northern Africa; July to November in Southern Africa (*90*); January to April in South Asia and Southeast Asia, north of the Equator; and August to October in Southeast Asia, south of the Equator (*17*, *91*). We remove from these

biomass burning months the contribution of anthropogenic sources determined as the annual means of the monthly data that fall below the 75th percentile for the corresponding year. We refer to the resultant values as biomass burning data and the values below the 75th percentiles as nonbiomass burning or anthropogenic activity data. We also assess consistency in trend directions between biomass burning data obtained with our statistical approach and biomass burning activity as indicated by satellite-derived burned fraction. The burned fraction product that we use is the Global Fire Emissions Database (GFED) version 4.1 that includes improved detection of small fires (v4.1s; https://globalfiredata.org/pages/data/; last accessed 22 April 2021) (*92*). This is provided at 0.25° by 0.25° for 2005–2016. We calculate annual burned fraction over the 22 target cities by sampling GFEDv4.1s grid cells that overlap with the same sampling extent as the satellite observations and calculate trends in the biomass burning data, nonbiomass burning (anthropogenic activity) data, and annual burned fraction using the linear Theil-Sen median estimator (*93*, *94*). We use the robust Theil-Sen median estimator as it reduces the influence of temporal variability in the data on the trend estimates.

Trends in bottom-up estimates of anthropogenic emissions

Satellite observations of the relatively short-lived pollutants NO_2 (lifetime of ~6 hours against conversion to reservoir compounds), HCHO (lifetime of 2 to 3 hours), and NH_3 (lifetime of 2 to 15 hours) provide constraints on precursor emissions of NO_x, reactive NMVOCs, and NH_3 (*25*, *30*, *37*, *88*). We assess the representation of these in bottom-up estimates of anthropogenic emissions and characterize possible anthropogenic sources contributing to the observed trends using the $CEDS_{GBD\text{-}MAPS}$ inventory (https://doi.org/10.5281/zenodo.3754964; last accessed 20 March 2021) developed for the U.S. Health Effects Institute (HEI) Global Burden of Disease–Major Air Pollution Sources (GBD-MAPS) project. It extends the record of emissions of the original Community Emissions Data System (CEDS) inventory (*95*) from 1970–2014 to 1970–2017 and improves representation of regional emissions by updating activity data and emission factors with data from other global, regional, and national inventories (*96*). Anthropogenic emissions in $CEDS_{GBD\text{-}MAPS}$ are provided as monthly gridded (0.5° by 0.5°) values for 11 broad source sectors (*96*). We sum 16 of 23 NMVOC classes with atmospheric lifetimes of <2 days to represent reactive NMVOC emissions. We isolate annual total city emissions from $CEDS_{GBD\text{-}MAPS}$ by sampling grid cells in the same way as we do GFEDv4.1s burned fraction and calculate trends using the same Theil-Sen median estimator (*93*, *94*). Emissions of NO_x and reactive NMVOCs are compared to trends in OMI NO_2 and the reactive NMVOC component of OMI HCHO, respectively, for 2005–2017. Emissions of NH_3 are compared to trends from IASI NH_3 for 2008–2017.

Trends in population exposure to hazardous air pollutants

We determine trends in city population exposure to $PM_{2.5}$ and NO_2 by calculating annual city population pseudo-exposure to total column AOD and tropospheric column NO_2 using the standard population exposure (E_{pop}) formula

$$E_{pop} = \sum_{i=1}^{N} C \quad (1)$$

where N is the total population from the United Nations (UN) (*1*) for each tropical city in Fig. 1 and C is the annual mean of the nonlinear fit used in that city to estimate trends in total column AOD as proxy for surface $PM_{2.5}$ (Fig. 3) and in tropospheric column NO_2 as proxy for surface NO_2 (Fig. 2A). We calculate E_{pop} at the record start (2005) and end (2018) to estimate relative trends in exposure. This approach draws on our previous findings that trends in satellite observations of column values are consistent with trends in surface concentrations (AOD for surface $PM_{2.5}$ and tropospheric column NO_2 for surface NO_2), even for cities where seasonality in AOD and $PM_{2.5}$ are decoupled (*6*).

Premature mortality from exposure to ambient $PM_{2.5}$

We estimate the increase in premature mortality due to the increase in exposure to $PM_{2.5}$ using annual mean $PM_{2.5}$ calculated with the GEOS-Chem model at the midpoint (2012) of the time period that we use here (2005–2018) and a risk assessment model that relates $PM_{2.5}$ exposure to risk of premature mortality. A description and validation of GEOS-Chem $PM_{2.5}$ is in (*19*). Briefly, GEOS-Chem simulations were carried out at fine spatial scales of 0.5° by 0.67° (~50 km by 67 km) over Asia and Africa using a comprehensive suite of natural and anthropogenic emissions, dynamic meteorology, and detailed coupled gas and aerosol phase chemistry (*19*). We calculate mean $PM_{2.5}$ for 2012 in each city by sampling GEOS-Chem grid cells in the same way as we do GFEDv4.1s burned fraction and $CEDS_{GBD\text{-}MAPS}$. We then use these values with the trends in AOD (Fig. 3) as proxies for trends in surface $PM_{2.5}$ to determine concentrations of $PM_{2.5}$ in 2005 and 2018. The health risk assessment model that we use is from a recent meta-analysis (*79*) of cohort studies for people 15 years and older and covering more extensive geographies, a wider $PM_{2.5}$ concentration range, and more health end points than previous approaches (*19*, *79*). We use the health risk assessment model to calculate the fraction of all-cause premature deaths attributable to exposure to $PM_{2.5}$ in 2005 and 2018 using the GEOS-Chem and satellite AOD–derived $PM_{2.5}$ as input. We then convert this to the number of premature deaths attributable to exposure to $PM_{2.5}$ for people older than 14 years in each city in 2005 and 2018 using country-level age-specific baseline mortality rates from the GBD (*97*), population data for each city from the UN (*1*), and data on the proportion of the population in each country >14 years old from the World Bank (*98*). The difference in the resultant premature deaths then gives the change in premature mortality from 2005 to 2018 due to the combined effect of changes in exposure to $PM_{2.5}$, to population, and to baseline mortality rates. We also quantify the relative role of each of these factors as the log transform of the ratio of premature mortality obtained with each of these parameters held fixed at 2005 values to premature mortality due to the combination of all factors, as in (*81*).

SUPPLEMENTARY MATERIALS

Supplementary material for this article is available at https://science.org/doi/10.1126/sciadv.abm4435

REFERENCES AND NOTES

1. UN, 2018. World Urbanization Prospects: The 2018 revision, online edition; https://population.un.org/wup/Download/ [accessed 14 June 2021].
2. D. Hoornweg, K. Pope, Population predictions for the world's largest cities in the 21st century. *Environ. Urban.* **29**, 195–216 (2017).
3. R. M. Duren, C. E. Miller, Measuring the carbon emissions of megacities. *Nat. Clim. Change* **2**, 560–562 (2012).
4. M. Krzyzanowski, J. S. Apte, S. P. Bonjour, M. Brauer, A. Cohen, A. M. Prüss-Ustun, Air pollution in the mega-cities. *Curr. Envir. Health Rpt.* **1**, 185–191 (2014).

5. S. C. Fang, E. G. Rodrigues, D. C. Christiani, Environmental health hazards in the tropics, in *Hunter's Tropical Medicine and Emerging Infectious Diseases*, E. T. Ryan, D. R. Hill, T. Solomon, N. E. Aronson, T. P. Endy, Eds. (Elsevier, ed. 10, 2020), pp. 200–208.
6. K. Vohra, E. A. Marais, S. Suckra, L. Kramer, W. J. Bloss, R. Sahu, A. Gaur, S. N. Tripathi, M. Van Damme, L. Clarisse, P. F. Coheur, Long-term trends in air quality in major cities in the UK and India: A view from space. *Atmos. Chem. Phys.* **21**, 6275–6296 (2021).
7. S. Yin, X. F. Wang, X. R. Zhang, M. Guo, M. Miura, Y. Xiao, Influence of biomass burning on local air pollution in mainland Southeast Asia from 2001 to 2016. *Environ. Pollut.* **254**, 112949 (2019).
8. A. M. Aghedo, M. G. Schultz, S. Rast, The influence of African air pollution on regional and global tropospheric ozone. *Atmos. Chem. Phys.* **7**, 1193–1212 (2007).
9. C. L. Reddington, L. Conibear, C. Knote, B. Silver, Y. J. Li, C. K. Chan, S. R. Arnold, D. V. Spracklen, Exploring the impacts of anthropogenic emission sectors on $PM_{2.5}$ and human health in South and East Asia. *Atmos. Chem. Phys.* **19**, 11887–11910 (2019).
10. E. A. Marais, C. Wiedinmyer, Air quality impact of diffuse and inefficient combustion emissions in Africa (DICE-Africa). *Environ. Sci. Technol.* **50**, 10739–10745 (2016).
11. S. E. Bauer, U. Im, K. Mezuman, C. Y. Gao, Desert dust, industrialization, and agricultural fires: Health impacts of outdoor air pollution in Africa. *J. Geophys. Res. Atmos.* **124**, 4104–4120 (2019).
12. A. S. Bockarie, E. A. Marais, A. R. MacKenzie, Air pollution and climate forcing of the charcoal industry in Africa. *Environ. Sci. Technol.* **54**, 13429–13438 (2020).
13. E. A. Marais, D. J. Jacob, K. Wecht, C. Lerot, L. Zhang, K. Yu, T. P. Kurosu, K. Chance, B. Sauvage, Anthropogenic emissions in Nigeria and implications for atmospheric ozone pollution: A view from space. *Atmos. Environ.* **99**, 32–40 (2014).
14. N. Ojha, A. Sharma, M. Kumar, I. Girach, T. U. Ansari, S. K. Sharma, N. Singh, A. Pozzer, S. S. Gunthe, On the widespread enhancement in fine particulate matter across the Indo-Gangetic Plain towards winter. *Sci. Rep.* **10**, 5862 (2020).
15. A. M. Thompson, W. K. Tao, K. E. Pickering, J. R. Scala, J. Simpson, Tropical deep convection and ozone formation. *B. Am. Meteorol. Soc.* **78**, 1043–1054 (1997).
16. J. E. Hickman, N. Andela, K. Tsigaridis, C. Galy-Lacaux, M. Ossohou, S. E. Bauer, Reductions in NO_2 burden over north equatorial Africa from decline in biomass burning in spite of growing fossil fuel use, 2005 to 2017. *Proc. Natl. Acad. Sci. U.S.A.* **118**, e2002579 (2021).
17. P. Bhardwaj, M. Naja, R. Kumar, H. C. Chandola, Seasonal, interannual, and long-term variabilities in biomass burning activity over South Asia. *Environ. Sci. Pollut. R.* **23**, 4397–4410 (2016).
18. GBD 2017 Risk Factor Collaborators, Global, regional, and national comparative risk assessment of 84 behavioural, environmental and occupational, and metabolic risks or clusters of risks for 195 countries and territories, 1990–2017: A systematic analysis for the Global Burden of Disease Study 2017. *Lancet* **392**, 1923–1994 (2018).
19. K. Vohra, A. Vodonos, J. Schwartz, E. A. Marais, M. P. Sulprizio, L. J. Mickley, Global mortality from outdoor fine particle pollution generated by fossil fuel combustion: Results from GEOS-Chem. *Environ. Res.* **195**, 110754 (2021).
20. Health Effects Institute, State of Global Air 2020. Special Report (Health Effects Institute, 2020).
21. World Bank, World Development Indicators (2019); https://databank.worldbank.org/source/world-development-indicators [accessed 14 June 2021].
22. R. V. Martin, M. Brauer, A. van Donkelaar, G. Shaddick, U. Narain, S. Dey, No one knows which city has the highest concentration of fine particulate matter. *Atmos. Environ. X* **3**, 100040 (2019).
23. M. Brauer, S. K. Guttikunda, K. Nishad, S. Dey, S. N. Tripathi, C. Weagle, R. V. Martin, Examination of monitoring approaches for ambient air pollution: A case study for India. *Atmos. Environ.* **216**, 116940 (2019).
24. R. Sahu, A. Nagal, K. K. Dixit, H. Unnibhavi, S. Mantravadi, S. Nair, Y. Simmhan, B. Mishra, R. Zele, R. Sutaria, V. M. Motghare, P. Kar, S. N. Tripathi, Robust statistical calibration and characterization of portable low-cost air quality monitoring sensors to quantify real-time O_3 and NO_2 concentrations in diverse environments. *Atmos. Meas. Tech.* **14**, 37–52 (2021).
25. B. N. Duncan, L. N. Lamsal, A. M. Thompson, Y. Yoshida, Z. F. Lu, D. G. Streets, M. M. Hurwitz, K. E. Pickering, A space-based, high-resolution view of notable changes in urban NO_x pollution around the world (2005–2014). *J. Geophys. Res. Atmos.* **121**, 976–996 (2016).
26. M. Van Damme, L. Clarisse, B. Franco, M. A. Sutton, J. W. Erisman, R. W. Kruit, M. van Zanten, S. Whitburn, J. Hadji-Lazaro, D. Hurtmans, C. Clerbaux, P. F. Coheur, Global, regional and national trends of atmospheric ammonia derived from a decadal (2008–2018) satellite record. *Environ. Res. Lett.* , 005017 (2021).
27. A. Hilboll, A. Richter, J. P. Burrows, Long-term changes of tropospheric NO_2 over megacities derived from multiple satellite instruments. *Atmos. Chem. Phys.* **13**, 4145–4169 (2013).
28. P. Alpert, O. Shvainshtein, P. Kishcha, AOD trends over megacities based on space monitoring using MODIS and MISR. *Am. J. Clim. Change* **01**, 117–131 (2012).
29. I. De Smedt, T. Stavrakou, J. F. Muller, R. J. van der A, M. Van Roozendael, Trend detection in satellite observations of formaldehyde tropospheric columns. *Geophys. Res. Lett.* **37**, L18808 (2010).
30. E. A. Marais, D. J. Jacob, T. P. Kurosu, K. Chance, J. G. Murphy, C. Reeves, G. Mills, S. Casadio, D. B. Millet, M. P. Barkley, F. Paulot, J. Mao, Isoprene emissions in Africa inferred from OMI observations of formaldehyde columns. *Atmos. Chem. Phys.* **12**, 6219–6235 (2012).
31. P. Lalitaporn, G. Kurata, Y. Matsuoka, N. Thongboonchoo, V. Surapipith, Long-term analysis of NO_2, CO, and AOD seasonal variability using satellite observations over Asia and intercomparison with emission inventories and model. *Air Qual. Atmos. Health* **6**, 655–672 (2013).
32. S. D. A. Kusumaningtyas, E. Aldrian, T. Wati, D. Atmoko, S. Sunaryo, The recent state of ambient air quality in Jakarta. *Aerosol Air Qual. Res.* **18**, 2343–2354 (2018).
33. P. Schneider, W. A. Lahoz, R. van der A, Recent satellite-based trends of tropospheric nitrogen dioxide over large urban agglomerations worldwide. *Atmos. Chem. Phys.* **15**, 1205–1220 (2015).
34. A. K. Georgoulias, R. J. van der A, P. Stammes, K. F. Boersma, H. J. Eskes, Trends and trend reversal detection in 2 decades of tropospheric NO_2 satellite observations. *Atmos. Chem. Phys.* **19**, 6269–6294 (2019).
35. J. Lelieveld, S. Beirle, C. Hormann, G. Stenchikov, T. Wagner, Abrupt recent trend changes in atmospheric nitrogen dioxide over the Middle East. *Sci. Adv.* **1**, e1500498 (2015).
36. L. Clarisse, M. Van Damme, C. Clerbaux, P. F. Coheur, Tracking down global NH_3 point sources with wind-adjusted superresolution. *Atmos. Meas. Tech.* **12**, 5457–5473 (2019).
37. M. Van Damme, L. Clarisse, S. Whitburn, J. Hadji-Lazaro, D. Hurtmans, C. Clerbaux, P. F. Coheur, Industrial and agricultural ammonia point sources exposed. *Nature* **564**, 99–103 (2018).
38. C. Li, R. V. Martin, A. van Donkelaar, B. L. Boys, M. S. Hammer, J. W. Xu, E. A. Marais, A. Reff, M. Strum, D. A. Ridley, M. Crippa, M. Brauer, Q. Zhang, Trends in chemical composition of global and regional population-weighted fine particulate matter estimated for 25 years. *Environ. Sci. Technol.* **51**, 11185–11195 (2017).
39. S. Provencal, P. Kishcha, A. M. da Silva, E. Elhacham, P. Alpert, AOD distributions and trends of major aerosol species over a selection of the world's most populated cities based on the 1st version of NASA's MERRA Aerosol Reanalysis. *Urban Clim.* **20**, 168–191 (2017).
40. T. Wang, Y. Song, Z. Xu, M. Liu, T. Xu, W. Liao, L. Yin, X. Cai, L. Kang, H. Zhang, T. Zhu, Why is the Indo-Gangetic Plain the region with the largest NH_3 column in the globe during pre-monsoon and monsoon seasons? *Atmos. Chem. Phys.* **20**, 8727–8736 (2020).
41. C. Li, C. McLinden, V. Fioletov, N. Krotkov, S. Carn, J. Joiner, D. Streets, H. He, X. R. Ren, Z. Q. Li, R. R. Dickerson, India is overtaking China as the world's largest emitter of anthropogenic sulfur dioxide. *Sci. Rep.* **7**, 14304 (2017).
42. S. S. Gunthe, P. F. Liu, U. Panda, S. S. Raj, A. Sharma, E. Darbyshire, E. Reyes-Villegas, J. Allan, Y. Chen, X. Wang, S. J. Song, M. L. Pohlker, L. H. Shi, Y. Wang, S. M. Kommula, T. J. Liu, R. Ravikrishna, G. McFiggans, L. J. Mickley, S. T. Martin, U. Poschl, M. O. Andreae, H. Coe, Enhanced aerosol particle growth sustained by high continental chlorine emission in India. *Nat. Geosci.* **14**, 77–84 (2021).
43. D. Hoornweg, P. Bhada-Tata, C. Kennedy, Environment: Waste production must peak this century. *Nature* **502**, 615–617 (2013).
44. R. T. Xu, S. F. Pan, J. Chen, G. S. Chen, J. Yang, S. R. S. Dangal, J. P. Shepard, H. Q. Tian, Half-century ammonia emissions from agricultural systems in Southern Asia: Magnitude, spatiotemporal patterns, and implications for human health. *Geohealth* **2**, 40–53 (2018).
45. S. K. Sharma, G. Kotnala, T. K. Mandal, Spatial variability and sources of atmospheric ammonia in India: A review. *Aerosol Sci. Eng.* **4**, 1–8 (2020).
46. J. Kuttippurath, A. Singh, S. P. Dash, N. Mallick, C. Clerbaux, M. Van Damme, L. Clarisse, P. F. Coheur, S. Raj, K. Abbhishek, H. Varikoden, Record high levels of atmospheric ammonia over India: Spatial and temporal analyses. *Sci. Total Environ.* **740**, 139986 (2020).
47. N. Damanik, H. C. Ong, C. W. Tong, T. M. I. Mahlia, A. S. Silitonga, A review on the engine performance and exhaust emission characteristics of diesel engines fueled with biodiesel blends. *Environ. Sci. Pollut. R.* **25**, 15307–15325 (2018).
48. Statista, Biodiesel consumption in Indonesia 2010–2020 (2021); www.statista.com/statistics/1055635/indonesia-biodiesel-consumption/ [accessed 25 June 2021].
49. P. Sicard, A. Anav, A. De Marco, E. Paoletti, Projected global ground-level ozone impacts on vegetation under different emission and climate scenarios. *Atmos. Chem. Phys.* **17**, 12177–12196 (2017).
50. F. Hayes, H. Harmens, K. Sharps, A. Radbourne, Ozone dose-response relationships for tropical crops reveal potential threat to legume and wheat production, but not to millets. *Sci. Afr.* **9**, e00482 (2020).
51. B. C. McDonald, J. A. de Gouw, J. B. Gilman, S. H. Jathar, A. Akherati, C. D. Cappa, J. L. Jimenez, J. Lee-Taylor, P. L. Hayes, S. A. McKeen, Y. Y. Cui, S. W. Kim, D. R. Gentner, G. Isaacman-VanWertz, A. H. Goldstein, R. A. Harley, G. J. Frost, J. M. Roberts, T. B. Ryerson, M. Trainer, Volatile chemical products emerging as largest petrochemical source of urban organic emissions. *Science* **359**, 760–764 (2018).
52. P. Gupta, S. A. Christopher, J. Wang, R. Gehrig, Y. Lee, N. Kumar, Satellite remote sensing of particulate matter and air quality assessment over global cities. *Atmos. Environ.* **40**, 5880–5892 (2006).

53. A. van Donkelaar, R. V. Martin, M. Brauer, B. L. Boys, Use of satellite observations for long-term exposure assessment of global concentrations of fine particulate matter. *Environ. Health Persp.* **123**, 135–143 (2015).
54. A. van Donkelaar, R. V. Martin, M. Brauer, N. C. Hsu, R. A. Kahn, R. C. Levy, A. Lyapustin, A. M. Sayer, D. M. Winker, Global estimates of fine particulate matter using a combined geophysical-statistical method with information from satellites, models, and monitors. *Environ. Sci. Technol.* **50**, 3762–3772 (2016).
55. G. Shaddick, M. L. Thomas, H. Amini, D. Broday, A. Cohen, J. Frostad, A. Green, S. Gumy, Y. Liu, R. V. Martin, A. Pruss-Ustun, D. Simpson, A. van Donkelaar, M. Brauer, Data integration for the assessment of population exposure to ambient air pollution for Global Burden of Disease assessment. *Environ. Sci. Technol.* **52**, 9069–9078 (2018).
56. A. Farahat, Comparative analysis of MODIS, MISR, and AERONET climatology over the Middle East and North Africa. *Ann. Geophys.* **37**, 49–64 (2019).
57. M. S. Hammer, A. van Donkelaar, C. Li, A. Lyapustin, A. M. Sayer, N. C. Hsu, R. C. Levy, M. J. Garay, O. V. Kalashnikova, R. A. Kahn, M. Brauer, J. S. Apte, D. K. Henze, L. Zhang, Q. Zhang, B. Ford, J. R. Pierce, R. V. Martin, Global estimates and long-term trends of fine particulate matter concentrations (1998–2018). *Environ. Sci. Technol.* **54**, 7879–7890 (2020).
58. Z. Hu, Q. Jin, Y. Ma, B. Pu, Z. Ji, Y. Wang, W. Dong, Temporal evolution of aerosols and their extreme events in polluted Asian regions during Terra's 20-year observations. *Remote Sens. Environ.* **263**, 112541 (2021).
59. S. A. Logothetis, V. Salamalikis, A. Gkikas, S. Kazadzis, V. Amiridis, A. Kazantzidis, 15-year variability of desert dust optical depth on global and regional scales. *Atmos. Chem. Phys.* **21**, 16499–16529 (2021).
60. M. Santoso, D. D. Lestiani, E. Damastuti, S. Kurniawati, I. Kusmartini, D. P. D. Atmodjo, D. K. Sari, T. Muhtarom, D. A. Permadi, P. K. Hopke, Long term characteristics of atmospheric particulate matter and compositions in Jakarta, Indonesia. *Atmos. Pollut. Res.* **11**, 2215–2225 (2020).
61. S. N. Koplitz, D. J. Jacob, M. P. Sulprizio, L. Myllyvirta, C. Reid, Burden of disease from rising coal-fired power plant emissions in Southeast Asia. *Environ. Sci. Technol.* **51**, 1467–1476 (2017).
62. R. R. Buchholz, H. M. Worden, M. Park, G. Francis, M. N. Deeter, D. P. Edwards, L. K. Emmons, B. Gaubert, J. Gille, S. Martinez-Alonso, W. F. Tang, R. Kumar, J. R. Drummond, C. Clerbaux, M. George, P. F. Coheur, D. Hurtmans, K. W. Bowman, M. Luo, V. H. Payne, J. R. Worden, M. Chin, R. C. Levy, J. Warner, Z. G. Wei, S. S. Kulawik, Air pollution trends measured from Terra: CO and AOD over industrial, fire-prone, and background regions. *Remote Sens. Environ.* **256**, 112275 (2021).
63. F. K. Dwomoh, M. C. Wimberly, Fire regimes and forest resilience: Alternative vegetation states in the West African tropics. *Landsc. Ecol.* **32**, 1849–1865 (2017).
64. E. E. McDuffie, R. V. Martin, J. V. Spadaro, R. Burnett, S. J. Smith, P. O'Rourke, M. S. Hammer, A. van Donkelaar, L. Bindle, V. Shah, L. Jaeglé, G. Luo, F. Yu, J. A. Adeniran, J. Lin, M. Brauer, Source sector and fuel contributions to ambient $PM_{2.5}$ and attributable mortality across multiple spatial scales. *Nat. Commun.* **12**, 3594 (2021).
65. J. L. Laughner, R. C. Cohen, Direct observation of changing NO_x lifetime in North American cities. *Science* **366**, 723–727 (2019).
66. R. F. Silvern, D. J. Jacob, L. J. Mickley, M. P. Sulprizio, K. R. Travis, E. A. Marais, R. C. Cohen, J. L. Laughner, S. Choi, J. Joiner, L. N. Lamsal, Using satellite observations of tropospheric NO_2 columns to infer long-term trends in US NO_x emissions: The importance of accounting for the free tropospheric NO_2 background. *Atmos. Chem. Phys.* **19**, 8863–8878 (2019).
67. Y. Z. Zhang, D. J. Jacob, X. Lu, J. D. Maasakkers, T. R. Scarpelli, J. X. Sheng, L. Shen, Z. Qu, M. P. Sulprizio, J. F. Chang, A. A. Bloom, S. Ma, J. Worden, R. J. Parker, H. Boesch, Attribution of the accelerating increase in atmospheric methane during 2010–2018 by inverse analysis of GOSAT observations. *Atmos. Chem. Phys.* **21**, 3643–3666 (2021).
68. T. S. Jayne, P. A. Sanchez, Agricultural productivity must improve in sub-Saharan Africa. *Science* **372**, 1045–1047 (2021).
69. S. Kaza, L. Yao, P. Bhada-Tata, F. Van Woerden, What a waste 2.0: A global snapshot of solid waste management to 2050 (World Bank, 2018); https://datatopics.worldbank.org/what-a-waste/trends_in_solid_waste_management.html.
70. Reuters, Kenya's Mombasa port shows growth, increased efficiency (2015); www.reuters.com/article/ozabs-uk-kenya-ports-idAFKCN0QP0OQ20150820 [accessed 1 July 2021].
71. R. Burnett, H. Chen, M. Szyszkowicz, N. Fann, B. Hubbell, C. A. Pope, J. S. Apte, M. Brauer, A. Cohen, S. Weichenthal, J. Coggins, Q. Di, B. Brunekreef, J. Frostad, S. S. Lim, H. D. Kan, K. D. Walker, G. D. Thurston, R. B. Hayes, C. C. Lim, M. C. Turner, M. Jerrett, D. Krewski, S. M. Gapstur, W. R. Diver, B. Ostro, D. Goldberg, D. L. Crouse, R. V. Martin, P. Peters, L. Pinault, M. Tjepkema, A. Donkelaar, P. J. Villeneuve, A. B. Miller, P. Yin, M. G. Zhou, L. J. Wang, N. A. H. Janssen, M. Marra, R. W. Atkinson, H. Tsang, Q. Thach, J. B. Cannon, R. T. Allen, J. E. Hart, F. Laden, G. Cesaroni, F. Forastiere, G. Weinmayr, A. Jaensch, G. Nagel, H. Concin, J. V. Spadaro, Global estimates of mortality associated with long-term exposure to outdoor fine particulate matter. *Proc. Natl. Acad. Sci. U.S.A.* **115**, 9592–9597 (2018).
72. D. M. Stieb, R. Berjawi, M. Emode, C. Zheng, D. Salama, R. Hocking, N. Lyrette, C. Matz, E. Lavigne, H. H. Shin, Systematic review and meta-analysis of cohort studies of long term outdoor nitrogen dioxide exposure and mortality. *PLOS ONE* **16**, e0246451 (2021).
73. M. Cacciottolo, X. Wang, I. Driscoll, N. Woodward, A. Saffari, J. Reyes, M. L. Serre, W. Vizuete, C. Sioutas, T. E. Morgan, M. Gatz, H. C. Chui, S. A. Shumaker, S. M. Resnick, M. A. Espeland, C. E. Finch, J. C. Chen, Particulate air pollutants, APOE alleles and their contributions to cognitive impairment in older women and to amyloidogenesis in experimental models. *Transl. Psychiatry* **7**, e1022 (2017).
74. S. Y. L. Chua, A. Warwick, T. Peto, K. Balaskas, A. T. Moore, C. Reisman, P. Desai, A. J. Lotery, B. Dhillon, P. T. Khaw, C. G. Owen, A. P. Khawaja, P. J. Foster, P. J. Patel, U. K. B. Eye, C. Vision, Association of ambient air pollution with age-related macular degeneration and retinal thickness in UK Biobank. *Br. J. Ophthalmol.* bjophthalmol-2020-316218 (2021).
75. Q. Li, D. N. Zheng, Y. Y. Wang, R. Li, H. P. Wu, S. X. Xu, Y. F. Kang, Y. X. Cao, X. J. Chen, Y. M. Zhu, S. G. Xu, Z. J. Chen, P. Liu, J. Qiao, Association between exposure to airborne particulate matter less than 2.5 μm and human fecundity in China. *Environ. Int.* **146**, 106231 (2021).
76. D. E. Schraufnagel, J. R. Balmes, C. T. Cowl, S. De Matteis, S. H. Jung, K. Mortimer, R. Perez-Padilla, M. B. Rice, H. Riojas-Rodriguez, A. Sood, G. D. Thurston; T. To, A. Vanker, D. J. Wuebbles, Air pollution and noncommunicable diseases: A review by the Forum of International Respiratory Societies' Environmental Committee, part 1: The damaging effects of air pollution. *Chest* **155**, 409–416 (2019).
77. X. Zhang, X. Chen, X. B. Zhang, The impact of exposure to air pollution on cognitive performance. *Proc. Natl. Acad. Sci. U.S.A.* **115**, 9193–9197 (2018).
78. R. W. Atkinson, B. K. Butland, H. R. Anderson, R. L. Maynard, Long-term concentrations of nitrogen dioxide and mortality a meta-analysis of cohort studies. *Epidemiology* **29**, 460–472 (2018).
79. A. Vodonos, Y. Abu Awad, J. Schwartz, The concentration-response between long-term $PM_{2.5}$ exposure and mortality; A meta-regression approach. *Environ. Res.* **166**, 677–689 (2018).
80. J. Lelieveld, C. Barlas, D. Giannadaki, A. Pozzer, Model calculated global, regional and megacity premature mortality due to air pollution. *Atmos. Chem. Phys.* **13**, 7023–7037 (2013).
81. V. A. Southerland, M. Brauer, A. Mohegh, M. S. Hammer, A. van Donkelaar, R. V. Martin, J. S. Apte, S. C. Anenberg, Global urban temporal trends in fine particulate matter (PM2·5) and attributable health burdens: Estimates from global datasets. *Lancet Planet. Health* **6**, e139–e146 (2022).
82. S. C. Anenberg, P. Achakulwisut, M. Brauer, D. Moran, J. S. Apte, D. K. Henze, Particulate matter-attributable mortality and relationships with carbon dioxide in 250 urban areas worldwide. *Sci. Rep.* **9**, 11552 (2019).
83. R. Burnett, C. A. Pope, M. Ezzati, C. Olives, S. S. Lim, S. Mehta, H. H. Shin, G. Singh, B. Hubbell, M. Brauer, H. R. Anderson, K. R. Smith, J. R. Balmes, N. G. Bruce, H. D. Kan, F. Laden, A. Pruss-Ustun, C. T. Michelle, S. M. Gapstur, W. R. Diver, A. Cohen, An integrated risk function for estimating the global burden of disease attributable to ambient fine particulate matter exposure. *Environ. Health Persp.* **122**, 397–403 (2014).
84. E. A. Marais, R. F. Silvern, A. Vodonos, E. Dupin, A. S. Bockarie, L. J. Mickley, J. Schwartz, Air quality and health impact of future fossil fuel use for electricity generation and transport in Africa. *Environ. Sci. Technol.* **53**, 13524–13534 (2019).
85. M. A. Ullah, A. Moin, Y. Araf, A. R. Bhuiyan, M. D. Griffiths, D. Gozal, Potential effects of the COVID-19 pandemic on future birth rate. *Front. Public Health* **8**, 578438 (2020).
86. A. Aassve, N. Cavalli, L. Mencarini, S. Plach, M. L. Bacci, The COVID-19 pandemic and human fertility. *Science* **369**, 370–371 (2020).
87. R. J. van der A, D. H. M. U. Peters, H. Eskes, K. F. Boersma, M. Van Roozendael, I. De Smedt, H. M. Kelder, Detection of the trend and seasonal variation in tropospheric NO_2 over China. *J. Geophys. Res. Atmos.* **111**, D12317 (2006).
88. V. Shah, D. J. Jacob, K. Li, R. F. Silvern, S. X. Zhai, M. Y. Liu, J. T. Lin, Q. Zhang, Effect of changing NO_x lifetime on the seasonality and long-term trends of satellite-observed tropospheric NO_2 columns over China. *Atmos. Chem. Phys.* **20**, 1483–1495 (2020).
89. C. Liousse, E. Assamoi, P. Criqui, C. Granier, R. Rosset, Explosive growth in African combustion emissions from 2005 to 2030. *Environ. Res. Lett.* **9**, 035003 (2014).
90. P. M. Barbosa, D. Stroppiana, J. M. Gregoire, J. M. C. Pereira, An assessment of vegetation fire in Africa (1981–1991): Burned areas, burned biomass, and atmospheric emissions. *Global Biogeochem. Cy.* **13**, 933–950 (1999).
91. K. P. Vadrevu, K. Lasko, L. Giglio, C. Justice, Vegetation fires, absorbing aerosols and smoke plume characteristics in diverse biomass burning regions of Asia. *Environ. Res. Lett.* **10**, 105003 (2015).
92. L. Giglio, J. T. Randerson, G. R. van der Werf, Analysis of daily, monthly, and annual burned area using the fourth-generation global fire emissions database (GFED4). *J. Geophys. Res. Biogeo.* **118**, 317–328 (2013).
93. P. K. Sen, Estimates of the regression coefficient based on Kendall's Tau. *J. Am.Stat. Assoc.* **63**, 1379–1389 (1968).
94. H. Theil, A rank-invariant method of linear and polynomial regression analysis. *Proc. K. Ned. Akad. Wet. Series A* **53**, 386–392 (1950).

95. R. M. Hoesly, S. J. Smith, L. Y. Feng, Z. Klimont, G. Janssens-Maenhout, T. Pitkanen, J. J. Seibert, L. Vu, R. J. Andres, R. M. Bolt, T. C. Bond, L. Dawidowski, N. Kholod, J. Kurokawa, M. Li, L. Liu, Z. F. Lu, M. C. P. Moura, P. R. O'Rourke, Q. Zhang, Historical (1750–2014) anthropogenic emissions of reactive gases and aerosols from the Community Emissions Data System (CEDS). *Geosci. Model Dev.* **11**, 369–408 (2018).
96. E. E. McDuffie, S. J. Smith, P. O'Rourke, K. Tibrewal, C. Venkataraman, E. A. Marais, B. Zheng, M. Crippa, M. Brauer, R. V. Martin, A global anthropogenic emission inventory of atmospheric pollutants from sector- and fuel-specific sources (1970-2017): An application of the Community Emissions Data System (CEDS). *Earth Syst. Sci. Data* **12**, 3413–3442 (2020).
97. Global Burden of Disease Collaborative Network, GBD 2019 Under-5 Mortality and Adult Mortality 1950–2019. Seattle, United States of America: Institute for Health Metrics and Evaluation (IHME) (2020).
98. World Bank, Population ages (2021); https://data.worldbank.org/topic/health?view=chart [accessed 24 August 2021].
99. P. Zoogman, D. J. Jacob, K. Chance, L. Zhang, P. Le Sager, A. M. Fiore, A. Eldering, X. Liu, V. Natraj, S. S. Kulawik, Ozone air quality measurement requirements for a geostationary satellite mission. *Atmos. Environ.* **45**, 7143–7150 (2011).
100. R. V. Martin, A. M. Fiore, A. Van Donkelaar, Space-based diagnosis of surface ozone sensitivity to anthropogenic emissions. *Geophys. Res. Lett.* **31**, L06120 (2004).
101. B. N. Duncan, Y. Yoshida, J. R. Olson, S. Sillman, R. V. Martin, L. Lamsal, Y. T. Hu, K. E. Pickering, C. Retscher, D. J. Allen, J. H. Crawford, Application of OMI observations to a space-based indicator of NO_x and VOC controls on surface ozone formation. *Atmos. Environ.* **44**, 2213–2223 (2010).
102. X. M. Jin, A. M. Fiore, L. T. Murray, L. C. Valin, L. N. Lamsal, B. Duncan, K. Folkert Boersma, I. De Smedt, G. G. Abad, K. Chance, G. S. Tonnesen, Evaluating a space-based indicator of surface ozone-NO_x-VOC sensitivity over midlatitude source regions and application to decadal trends. *J. Geophys. Res. Atmos.* **122**, 10439–10461 (2017).
103. A. H. Souri, Y. Choi, W. Jeon, J. H. Woo, Q. Zhang, J. Kurokawa, Remote sensing evidence of decadal changes in major tropospheric ozone precursors over East Asia. *J. Geophys. Res. Atmos.* **122**, 2474–2492 (2017).
104. A. H. Souri, C. R. Nowlan, G. M. Wolfe, L. N. Lamsal, C. E. C. Miller, G. G. Abad, S. J. Janz, A. Fried, D. R. Blake, A. J. Weinheimer, G. S. Diskin, X. Liu, K. Chance, Revisiting the effectiveness of $HCHO/NO_2$ ratios for inferring ozone sensitivity to its precursors using high resolution airborne remote sensing observations in a high ozone episode during the KORUS-AQ campaign. *Atmos. Environ.* **224**, 117341 (2020).
105. J. R. Schroeder, J. H. Crawford, A. Fried, J. Walega, A. Weinheimer, A. Wisthaler, M. Muller, T. Mikoviny, G. Chen, M. Shook, D. R. Blake, G. S. Tonnesen, New insights into the column CH2O/NO2ratio as an indicator of near-surface ozone sensitivity. *J. Geophys. Res. Atmos.* **122**, 8885–8907 (2017).

Acknowledgments

Funding: This work was funded by a University of Birmingham Global Challenges Studentship awarded to K.V., an NERC/EPSRC grant (EP/R513465/1) awarded to E.A.M., and the Wallace Global Fund. The ULB research by M.V.D., L.C., and P.-F.C. was supported by the Belgian State Federal Office for Scientific, Technical, and Cultural Affairs (Prodex arrangement IASI.FLOW) and the Air Liquide Foundation. L.C. is a research associate supported by the Belgian F.R.S.-FNRS. This publication was made possible by USEPA grant RD-835872. Its contents are solely the responsibility of the grantee and do not necessarily represent the official views of the USEPA. Furthermore, USEPA does not endorse the purchase of any commercial products or services mentioned in the publication. **Author contributions:** K.V. and E.A.M. designed the research, with input from W.J.B. J.S. and L.J.M. provided guidance on the health impact calculations and led the projects that generated GEOS-Chem output. New satellite data products were provided by M.V.D., L.C., and P.-F.C. K.V. analyzed the data. K.V. and E.A.M. wrote the paper, with input from all coauthors. **Competing interests:** The authors declare that they have no competing interests. **Data and materials availability:** Most data needed to evaluate the conclusions in the paper are present in the paper and/or the Supplementary Materials. IASI NH_3 data were provided by M.V.D., L.C., and P.-F.C. and are now available at https://iasi.aeris-data.fr/nh3/ (last accessed 10 April 2021). GEOS-Chem codes are available at the GEOS-Chem website (https://geos-chem.seas.harvard.edu/; last accessed 9 February 2021), and the GEOS-Chem output relevant to this work is available at https://doi.org/10.5522/04/17152679 (last accessed 9 December 2021). URLs and DOIs (if available) of the other data used in this study are given in Materials and Methods.

Submitted 17 September 2021
Accepted 18 February 2022
Published 8 April 2022
10.1126/sciadv.abm4435

ScienceAdvances

Rapid rise in premature mortality due to anthropogenic air pollution in fast-growing tropical cities from 2005 to 2018

Karn VohraEloise A. MaraisWilliam J. BlossJoel SchwartzLoretta J. MickleyMartin Van DammeLieven ClarissePierre-F. Coheur

Sci. Adv., 8 (14), eabm4435. • DOI: 10.1126/sciadv.abm4435

Science Advances (ISSN) is published by the American Association for the Advancement of Science. 1200 New York Avenue NW, Washington, DC 20005. The title *Science Advances* is a registered trademark of AAAS.